Registration of Brain Tumor Images using Hyper-elastic Regularization

Andac Hamamci, Gozde Unal

Abstract In this paper, we present a method to estimate a deformation field between two instances of a brain volume having tumor. The novelties include the assessment of the disease progress by observing the healthy tissue deformation and usage of the Neo-Hookean strain energy density model as a regularizer in deformable registration framework. Implementations on synthetic and patient data provide promising results, which might have relevant use in clinical problems.

1 Introduction

Registration of brain volumes with tumors is important to track the changes between two instances in order to assess the progression of the tumor and the treatment response. The first step is a rigid/affine registration between volumes. Although this is a challenging problem due to the changes caused by the tumor, various approaches on the problem reported successful results in the literature [4, 15, 13]. The total deformation caused by the tumor growth can be taught as the combination of infiltration to the healthy tissue and mass effect components. Our aim in this work is to separate the mass effect and infiltration components, so that, malignancy and the reversibility of the destruction can be determined. The healthy brain tissue in one of the images can be warped onto the other ignoring the tumor tissue regions, as the latter may contain uncertainty due to highly complex tumor growth and therapy processes. Hence, matching only the healthy tissues in baseline and follow-up tumor images provides an estimation of the intracranial pressure caused by the tumor growth plus the mass effect.

Faculty of Engineering and Natural Sciences, Sabanci University, Istanbul, Turkey e-mail: `gozdeunal@sabanciuniv.edu`

A similar problem arises in deformable registration of the brain with tumors to a healthy population atlas. The main difference to the intra-subject registration problem is that the deformation also includes inter-subject variations. Hence, a general strategy to solve this problem is to iterate the forward model by simulating the tumor growth on the atlas and refining the parameters of the simulation model by comparing it to the tumor image [6]. This requires strong models, which rely on realistic models of tumor growth and deformations due to the mass effect [6, 8, 2, 14]. The main problem with those approaches is that the growth of the tumor is mostly affected by the uncontrolled parameters such as treatment and requires sophisticated tumor growth models even without treatment. In "Geometric Metamorphosis" paper, Niethammer et.al, proposed an interesting approach to the problem using a weak model by separating the foreground, hence the tumor growth, and the background changes [11].
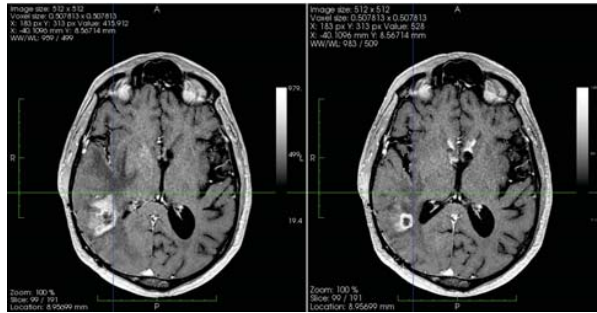

Fig. 1: A sample axial slice from baseline (on the right) and follow-up (on the left) MRI.

For the problem of intra-subject registration, our approach is based on the assumption that the deformations except around the tumor volume are caused by the mass effect of the tumor, hence obey the bio-mechanical rules. This is different from the atlas matching problem, since there is also inter-subject variations between the images. Sample baseline and follow-up MRI slices are shown in Figs. 1 and 2. Deformation of the ventricles and sulci due to the mass effect of the growing tumor can be clearly observed on the right hemisphere. Although, a mapping of the tumor tissue between the baseline and the follow-up is not well defined due to the uncertain growth pattern and therapy effects, a mapping between the healthy tissues can be estimated. Therefore, our aim is to find a mapping between the healthy tissues of the brains, which obeys the nonlinear elastic finite deformation models.

The results of the experimental studies on animals suggest to model the brain with a homogeneous hyper-viscoelastic non-isotropic material [9]. In the image analysis literature, simplified hyper-elastic or linear models are
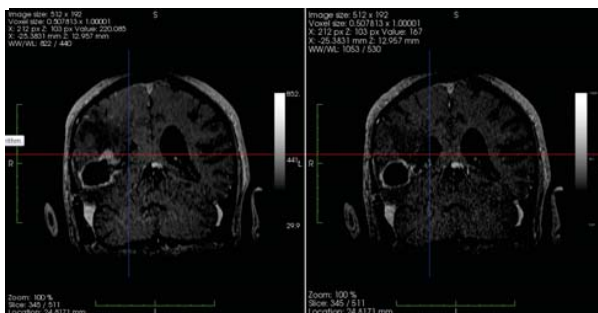
Fig. 2: A sample coronal slice from baseline (on the right) and follow-up (on the left) MRI.

used: Neo-Hookean [7], Ogden type [16, 10], Saint-Venant Kirchhoff model [18], linear elastic [3], linear viscoelastic type [2]. In their work, comparing viscoelastic, hyper-elastic and linear elastic models on brain simulations, Wittek et. al. reports no significant difference on the results obtained [17]. In "Nonlinear Elastic Registration with Unbiased Regularization in Three Dimensions", Saint-Venant Kirchhoff model was used as a regularizer in the registration of serial magnetic resonance images [18].

Our novel contributions in this paper are: (i) Matching healthy tissue to healthy tissue of the brain using a dedicated image data term; (ii) Using the hyper-elastic Neo-Hookean strain energy density as a regularizer in deformable registration framework; (iii) Derivation of displacement field update equations based on the Neo-Hookean model.

2 Methods

2.1 Background

The mechanical properties of a hyper-elastic material are characterized completely by a scalar strain-energy density function W. Specifying the strain energy density W as a function of deformation gradient tensor F: $W = W(F)$ ensures that the material is perfectly elastic. The general form of the strain energy density is guided by experiment [1].

Let us define the displacement field from the un-deformed to deformed configuration as $u : \Omega \longrightarrow \mathbb{R}^3$ where $\Omega \in \mathbb{R}^3$. In addition to the strain energy density $W = W(x, \nabla u)$, let $f = f(x, u(x))$ denote the external energy, then the equilibrium configurations can be determined as the minima of the total energy functional:

$$I(u) = \int_{\Omega} W(x, \nabla u) dx - \int_{\Omega} f(x, u) dx \qquad (1)$$

The Euler-Lagrange system associated with the functional I is precisely the equilibrium equations:

$$div(\frac{\partial W}{\partial F}(x, \nabla u(x))) + \frac{\partial f}{\partial u}(x, u(x)) = 0 \qquad (2)$$

where $F_{ij} = \sigma_{ij} + \frac{\partial u_i}{\partial x_j}$ and $\frac{\partial W}{\partial F}^T$ is called the First Piola-Kirchhoff tensor. Common constitutive hyper-elastic strain energy density models include [12]:

- St Venant-Kirchhoff material:

$$W(F) = \alpha(trE)^2 + \beta tr(E^2) \ \ where \ \ E = \frac{1}{2}(F^T F - I) \qquad (3)$$

- Neo-Hookean material:

$$W(F) = a\|F\|^2 + g(detF) \ \ where \ \ a > 0 \qquad (4)$$

2.2 Hyper-elastic Registration for Tumor Follow-up

Let R(x) and T(x) denote the brain tissue maps (White Matter + Gray Matter + Tumor) of reference (undeformed) and target (deformed) volumes respectively. We are assuming the mechanical properties of white matter and gray matter are similar. The problem is to find the displacement u from the volume R to T, which minimizes the given functional:

$$u^* = \arg\min_{u} \int_{\Omega} f(R(x), T(x - u(x))) + \alpha W(x, \nabla u) dx \qquad (5)$$

where f is the external energy density term calculated as a similarity measure between the two volumes and α is the weighting parameter of the regularizer term W.

Distance maps to the binary segmentations are used, instead of common image similarity measures, such as mutual information. In this way, state of the art segmentation methods specific to the problem could be used to obtain reliable image forces. Reliability of the image term is especially important for the proposed regularizer dominant approach.

2.3 Volumetric Data Term

Since a mapping between the two solid body is needed, all the displacements from the reference should point towards inside of the target body. This is ensured by the following external energy density term:

$$f_V(x, u(x)) = \chi_R(x) D_T(x + u(x)) \tag{6}$$

where χ_R is the indicator function of the reference body, with the value of 1 for the points inside and 0 for the outside. D_T is the distance function to the target body, where D_T is zero inside the target body and takes the distance values outside the target body. The goal is that the displacement vectors can move freely inside the target volume. To derive the Euler-Lagrange condition for this energy density, the derivative of the functional in Eq. 6 is written as:

$$\frac{\partial}{\partial u} f_V(x, u(x)) = \chi_R(x) \frac{\partial}{\partial u} D_T(x + u(x)) \tag{7}$$

This is simply the gradient of the distance function of the target body:

$$\frac{\partial}{\partial u} f_V(x, u(x)) = \chi_R(x) \nabla D_T(x + u(x)) \tag{8}$$

2.4 Boundary Data Term

In addition, a solution that matches the outside surfaces of the two bodies, is required. Therefore, another external energy density is added which penalizes the distance from the surface of the reference body to the surface of the target. We note that, displacement vectors can still move on the target surface freely. This is ensured by the following energy term:

$$f_B(x, u(x)) = \chi_{\partial R}(x) D_{\partial T}(x + u(x)) \tag{9}$$

where $\chi_{\partial R}$ is the indicator function of the boundary of the reference body, having the value of 1 for the points on the boundary and 0 elsewhere. $D_{\partial T}$ is the distance function to the boundary of the target body. The Euler-Lagrange condition for this energy density is:

$$\frac{\partial}{\partial u} f_B(x, u(x)) = \chi_{\partial R}(x) \frac{\partial}{\partial u} D_{\partial T}(x + u(x)) = \chi_{\partial R}(x) \nabla D_{\partial T}(x + u(x)) \tag{10}$$

2.5 Hyper-elastic Regularizer

For simplicity, assuming nonlinear hyper-elastic model in Ogden form as in [10]:

$$W = \frac{2\mu}{\alpha^2}(\bar{\lambda}_1{}^\alpha + \bar{\lambda}_2{}^\alpha + \bar{\lambda}_3{}^\alpha - 3) + \frac{1}{D_1}(J-1)^2 \qquad (11)$$

where principal strains $\bar{\lambda}_i = \lambda_i/J^{1/3}$, $\lambda_i = e_i^{1/2}$, e_i's are eigenvalues of $B = FF^T$, J is the determinant of the deformation $J = det(F)$ and deformation gradient tensor $F_{ij} = \frac{\partial u_i}{\partial x_j} + \delta_{ij}$. In [9], α parameter of the model for the brain tissue is determined as $\alpha = -4.7$. For simplicity, in this work we will use $\alpha = 2$, which is known as the Neo-Hookean model. By replacing $Tr(B) = \lambda_1^2 + \lambda_2^2 + \lambda_3^2$, the strain energy density function becomes:

$$W = \frac{\mu}{2}(\frac{Tr(B)}{J^{2/3}} - 3) + \frac{1}{D_1}(J-1)^2 \qquad (12)$$

Let us derive the Euler-Lagrange condition on the displacement field u for minimizing the given strain energy functional in terms of the trace and determinant. The derivative of the energy density W with respect to u_i is given by:

$$\nabla_{u_i} W = \frac{\partial W}{\partial u_i} - \sum_j \frac{\partial}{\partial x_j} \frac{\partial W}{\partial(\partial u_i/\partial x_j)} \qquad (13)$$

The first term drops, as the energy density functional W is not dependent on the u but its derivatives. The derivative with respect to $\partial u_i/\partial x_j$ is identical to the derivative with respect to F_{ij}, therefore, rewriting Eq. 13 results in:

$$\nabla_{u_i} W = - \sum_j \frac{\partial}{\partial x_j} \frac{\partial W}{\partial F_{ij}} \qquad (14)$$

Now, we need the derivatives $\frac{\partial W}{\partial F_{ij}}$, which is also known as the 1st Piola-Kirchhoff tensor in mechanics literature. After a set of manipulations, the following derivative is obtained:

$$\nabla_{u_i}W = -\frac{\mu}{J^{2/3}}\sum_j(\frac{\partial F}{\partial x_j})_{ij} + \frac{2\mu}{3J^{2/3}}\sum_j F_{ij}Tr(F^{-1}\frac{\partial F}{\partial x_j})$$
$$-(\frac{\mu Tr(B)}{3J^{2/3}} - \frac{2J(J-1)}{D1})\sum_j(F^{-1}\frac{\partial F}{\partial x_j}F^{-1})_{ji}$$
$$-(\frac{2\mu Tr(B)}{9J^{2/3}} + \frac{2J(2J-1)}{D1})\sum_j(F^{-1})_{ji}Tr(F^{-1}\frac{\partial F}{\partial x_j})$$
$$+\frac{2\mu}{3J^{2/3}}\sum_j(F^{-1})_{ji}Tr(\frac{\partial F}{\partial x_j}F^T)$$

$$(15)$$

2.6 Implementation Details

A multi-resolution approach is implemented to increase the convergence speed. Volumes are down-sampled using trilinear interpolation and the obtained displacement field is interpolated to the higher resolution at the end of each stage.

The update equation for the displacement field u is obtained by the gradient descent method as:

$$\frac{\partial u}{\partial t} = -(Eq.8 + Eq.10 + Eq.15) \tag{16}$$

If the maximum change due to the regularizer is greater than 1, the update of the displacement is normalized by dividing to the maximum update:

$$\nabla_u W = \begin{cases} \frac{\nabla_u W}{max(\nabla_u W)} & \text{if } \nabla_u W > 1 \\ \nabla_u W & otherwise \end{cases} \tag{17}$$

Scaling of the strain energy density function of the regularizer term is arbitrary. Therefore, instead of having two independent parameters μ and D_1 for the energy functional in Eq. 12, the algorithm is affected mainly by the ratio $\frac{\mu}{1/D_1} = \mu D_1$.

The effect of a μD_1 at a higher limit is shown on the sub-figure at the center of Fig. 4, which corresponds to the first term in Eq. 12, whereas, the effect of a zero μD_1 is shown on the right sub-figure of Fig. 4, which corresponds to the second term. In this work, our aim is to estimate the cause (tumor deformation) by observing the result (displacement at the boundaries). Therefore, we assure the reversibility by enforcing a highly incompressible behavior to prevent the energy to be stored in the material, which we can not observe by MRI. This is achieved by penalizing the local volume changes more by setting a low μD_1. We also assume that the total volume increase of the

brain parenchyma is mostly caused by the increase of the tumor volume. Therefore, by setting the tumor region as a hole for the regularizer, which does not contribute to the external energy, and using an incompressible strain energy density, the observed local volume changes at the boundaries of the parenchyma are carried to the tumor area. We also note that, by decreasing the μ, the dependence of the strain energy density to the model parameter α in Eq. 11 is decreased, which strengthen our simplification approach of using Neo-Hookean model ($\alpha = 2$) instead of Ogden form with $\alpha = -4.7$.

Starting with an initial time step δt for the regularizer, the value is halved if the strain energy is not decreased by updating the displacement field.

The first derivatives are calculated by using central difference finite differencing scheme as:

$$V_x(x, y, z) = \frac{V(x + h, y, z) - V(x - h, y, z)}{2h} \qquad (18)$$

The derivative $\frac{\partial F}{\partial x_j}$ is given by the following matrix:

$$\frac{\partial F}{\partial x_j} = \begin{pmatrix} \frac{\partial^2 u_1}{\partial x_1 \partial x_j} & \frac{\partial^2 u_1}{\partial x_2 \partial x_j} & \frac{\partial^2 u_1}{\partial x_3 \partial x_j} \\ \frac{\partial^2 u_2}{\partial x_1 \partial x_j} & \frac{\partial^2 u_2}{\partial x_2 \partial x_j} & \frac{\partial^2 u_2}{\partial x_3 \partial x_j} \\ \frac{\partial^2 u_3}{\partial x_1 \partial x_j} & \frac{\partial^2 u_3}{\partial x_2 \partial x_j} & \frac{\partial^2 u_3}{\partial x_3 \partial x_j} \end{pmatrix}$$

Its components are calculated by second order finite difference discretization as:

$$V_{xx}(x, y, z) = \frac{V(x - h, y, z) - 2V(x, y, z) + V(x + h, y, z)}{h^2}$$

$$V_{xy}(x, y, z) = \frac{V(x+h, y+h, z) - V(x+h, y-h, z) - V(x-h, y+h, z) + V(x-h, y-h, z)}{4h^2}$$

$$\qquad (19)$$

Other derivative components are calculated similarly. At the boundaries, one-sided differences are used, for both the first and the second order derivatives.

3 Experiments and Results

3.1 Regularizer Test

To test the regularizer initially, the algorithm is run on 10x10x10 mask on a 20x20x20 lattice with a single constant displacement vector (0.0001,0.0001,0.0) and zero boundary conditions. The central xy-plane of the input and the result obtained with $\mu = 0.8$ and $D_1 = 1.0$ is given in Fig. 3 with a closer look at Fig. 4. The effect of setting the parameters of the model at the lower

and higher limits is shown on the middle and the right sub-figures of Fig. 4. Although, incompressibility is a necessity for our problem as discussed in the method, setting a non-zero value to μ helps to increase the stability of the solution.
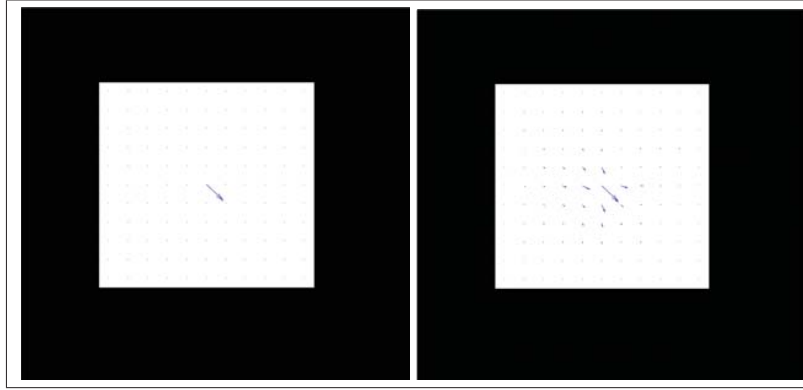

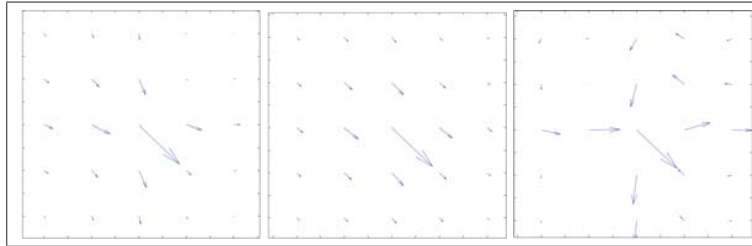Fig. 3: Left: Input phantom for the regularizer test. Right: Output of the regularizer test.

Fig. 4: Left: A closer view of the output of the regularizer test on phantom. Middle: The result obtained on phantom by increasing μ in the strain energy density model in Eq. 12. Right: The result obtained on phantom by setting the μ as zero in the strain energy density model in Eq. 12.

3.2 Phantom Results

To test the algorithm, two synthetic volumes are created as a sphere and an ellipsoid. Firstly, the method is run to determine the displacement field from sphere to ellipsoid by considering only the image terms, without the regularization. The results obtained with these external energies alone are shown in Fig. 5.
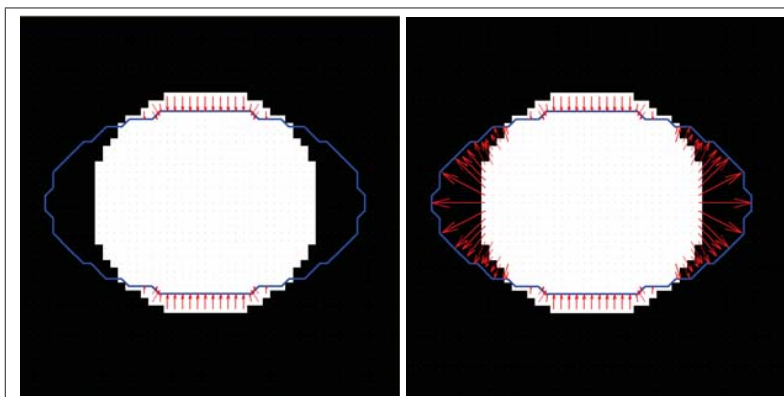

Fig. 5: The central slices of the results obtained on synthetic volumes by applying the volumetric data term only (on left) and boundary data term only (on right) without regularization.

The central xy-plane of the result obtained by considering both image terms and the regularizer with $\mu = 0.4$ and $D_1 = 1.0$ is given in Fig. 6. Since the target volume is larger than the reference, the incompressibility, enforced by a low μ, results curled field to minimize the change of the volume. Shortfall appearance of the vectors is due to the 2D slice visualization of the 3D vector field.

3.3 Experiments on MRI Brain Tumor Followup Volumes

3.3.1 The Data

MR images of a brain tumor patient (Glioblastoma Multiforme), obtained by 1.5T MRI scanner at high resolution ($\approx$ 0.5x0.5x1.0 mm) contiguous axial T1 weighted 3D SPGR (TE/TR = 3.16s/8.17s, FA=25) sequence acquired
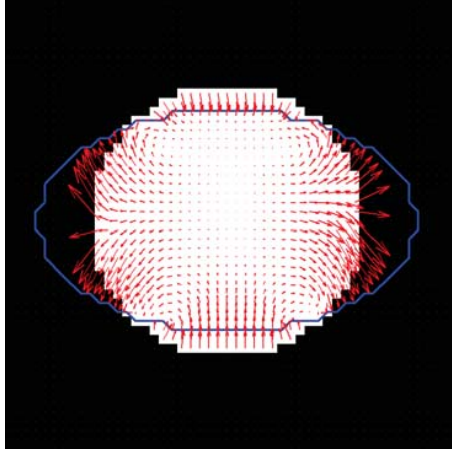
Fig. 6: The result obtained on the synthetic volumes. Reference spherical volume is labeled with white color, the blue contour represents the boundary of the target ellipsoid, and the displacement field from sphere to ellipsoid is indicated with arrows in red color.

after IV injection of 10cc 0.5M Multihance Gd, is used for validation study. The sample slices of the baseline and the follow-up volume, obtained 35 days after, are given in Fig. 1 and 2.

3.3.2 Preprocessing MRI Volumes

Statistical Parametric Mapping (SPM) software [1], distributed by Wellcome Trust Centre for Neuroimaging, London, which gives accurate results in brain volumes with tumors, is used for standard operations such as: rigid registration, segmentation and smoothing. Specifically, the following preprocessing operations are applied to the data before the execution of the deformable registration:

- Follow-up volume is registered to the baseline volume using co-register function of SPM8.
- White matter (WM) and gray matter (GM) segmentations ($P > 0.5$) are obtained for both volumes using SPM8.
- Tumors in both volumes are segmented using the Tumor-cut algorithm [5].
- For each of the volumes, Tumor, WM and GM segmentations are combined using: $\Omega_{Tumor} \cup \Omega_{WM} \cup \Omega_{GM}$.

---

[1] http://www.fil.ion.ucl.ac.uk/spm/

- Each combined binary volume is smoothed by smooth function of the SPM8 with a Gaussian kernel having 8x8x8mm full width at half maximum.
- Finally, binary maps are converted to isotropic voxels ($1x1x1mm$).

3.3.3 Results

Sample slices of the result obtained on tumor patient data is shown in Fig. 7. Intense displacement on the hemisphere with tumor, due to the mass effect, can be observed. At the bottom of the sub-figure on the right, displacement of the sulci due to the increased cerebrospinal fluid (CSF) pressure can be seen. Also, the increase in the CSF pressure results slight displacements at the ventricles of the healthy hemisphere, on the top. Displacement field, overlayed
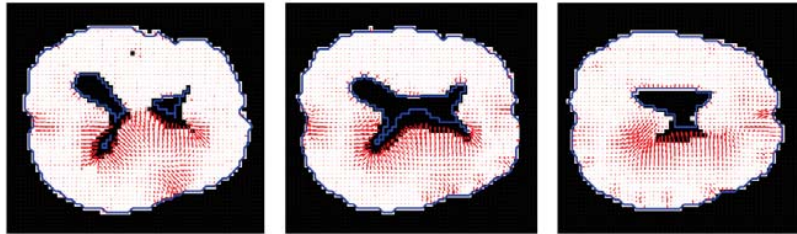

Fig. 7: Sample slices of the result obtained on tumor patient data in 3x3x3mm voxel size. Binarized brain tissue of the reference volume is labeled in white color, the blue contour indicates the boundary of the target volume, and the displacement field is indicated with arrows in red.

on a sample axial slice of the reference MRI in high resolution, is given in Fig. 8. The mass effect around the tumor is clearly observed. A closer look to the ventricle at the hemisphere without tumor depicts the displacement due to the expansion of the ventricle. When we focus on the displacement around the tumor as in Fig. 9, the displacement caused by the mass-effect (at the top) and the tumor growth (on the right) can be observed. The vectors at the the bottom-left of the tumor explains the local shrinkage of the tumor as a tissue displacement.

4 Discussion and Conclusions

A method to register the brain tissues in baseline and follow-up MRI volumes using finite deformation models is presented. Implementations on synthetic
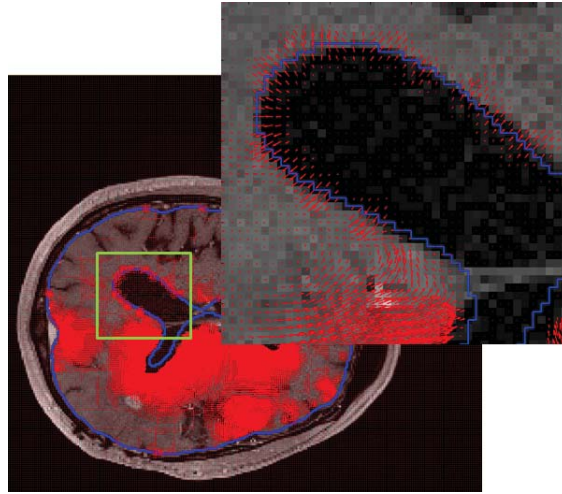
Fig. 8: Displacement field (in red) overlayed on a sample MRI slice of the reference volume, with the boundary of the target volume indicated with the blue contour. A closer look to the ventricle of the hemisphere without tumor.
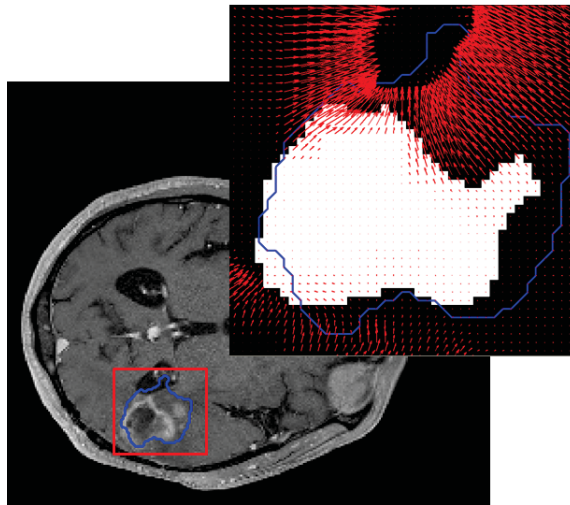

Fig. 9: A closer look to the tumor where the baseline tumor volume is labeled with white color, the follow-up tumor boundary is indicated with blue contour and the displacement field is overlayed with red arrows.

and patient data, with only minimal user interaction, provide promising results, which might have relevant use in clinical problems. Publicly available state-of-the-art algorithms for the rigid registration and tissue/tumor segmentation are able to provide highly accurate outputs, which is a necessity to obtain an accurate displacement field. Accuracy of the method could be increased by improving the data term, such as by adding vessel correspondences or manual landmarks.

References

[1] Bower AF (2010) Applied Mechanics of Solids. Taylor and Francis Group, LLC

[2] Clatz O, Sermesant M, Bondiau PY, Delingette H, Warfield S, Malandain G, Ayache N (2005) Realistic simulation of the 3d growth of brain tumors in mr images coupling diffusion with biomechanical deformation. IEEE Trans Med Imaging 24(10):1334–1346

[3] Davatzikos C (1997) Spatial transformation and registration of brain images using elastically deformable models. Computer Vision and Image Understanding 66(2):207 – 222

[4] Demir A, Unal G, Karaman K (2010) Anatomical landmark based registration of contrast enhanced t1-weighted mr images. In: Proceedings of the 4th international conference on Biomedical image registration, Springer-Verlag, Berlin, Heidelberg, WBIR'10, pp 91–103

[5] Hamamci A, Kucuk N, Karaman K, Engin K, Unal G (2012) Tumor-cut: Segmentation of brain tumors on contrast enhanced mr images for radiosurgery applications. Medical Imaging, IEEE Transactions on 31(3):790 –804

[6] Hogea C, Biros G, Abraham F, Davatzikos C (2007) A robust framework for soft tissue simulations with application to modeling brain tumor mass effect in 3d mr images. Physics in Medicine and Biology 52(23):6893

[7] Joldes GR, Wittek A, Miller K (2009) Suite of finite element algorithms for accurate computation of soft tissue deformation for surgical simulation. Medical Image Analysis 13(6):912 – 919

[8] Konukoglu E, Clatz O, Bondiau PY, Delingette H, Ayache N (2010) Extrapolating glioma invasion margin in brain magnetic resonance images: suggesting new irradiation margins. Medical Image Analysis 14(2):111–125

[9] Miller K, Chinzei K (2002) Mechanical properties of brain tissue in tension. Journal of Biomechanics 35(4):483 – 490

[10] Mohamed A, Davatzikos C (2005) Finite element modeling of brain tumor mass-effect from 3d medical images. In: Proceedings of the 8th international conference on Medical Image Computing and Computer-Assisted Intervention - Volume Part I, Springer-Verlag, Berlin, Heidelberg, MICCAI'05, pp 400–408

[11] Niethammer M, Hart G, Pace D, Aylward S (2011) Geometric metamorphosis. In: MICCAI

[12] Pedregal P (2000) Variational methods in nonlinear elasticity. Society for Industrial and Applied Mathematics, Philadelphia, PA, USA

[13] Periaswamy S, Farid H (2003) Elastic registration with partial data. Proc of Workshop on Biomedical Image Registration WBIR03 pp 102–111

[14] Prastawa M, Bullitt E, Gerig G (2009) Simulation of brain tumors in mr images for evaluation of segmentation efficacy. Medical Image Analysis 13(2):297 – 311

[15] Reuter M, Rosas HD, Fischl B (2010) Highly accurate inverse consistent registration: a robust approach. NeuroImage 53(4):1181–1196

[16] Wittek A, Miller K, Kikinis R, Warfield SK (2007) Patient-specific model of brain deformation: Application to medical image registration. Journal of Biomechanics 40(4):919 – 929

[17] Wittek A, Hawkins T, Miller K (2009) On the unimportance of constitutive models in computing brain deformation for image-guided surgery. Biomechanics and Modeling in Mechanobiology 8:77–84

[18] Yanovsky I, Le Guyader C, Leow A, Toga A W, Thompson P M, Vese L (2008) Unbiased Volumetric Registration via Nonlinear Elastic Regularization. In: Pennec X (ed) 2nd MICCAI Workshop on Mathematical Foundations of Computational Anatomy, New-York, États-Unis